

Charge decoherence in laterally coupled quantum dots due to electron-phonon interactions

V.N. Stavrou and Xuedong Hu

Department of Physics, State University of New York at Buffalo, New York 14260, USA

We have investigated electron charge decoherence in a laterally-coupled single-electron semiconductor double quantum dot through electron-phonon interaction. We analytically and numerically evaluated the relaxation and dephasing rates due to electron coupling to both acoustic and optical phonons, and explored the system parameter space in terms of interdot distance, strength of single-dot confinement, and inter-dot coupling strength. Our numerically results show that the electron scattering rates are strongly dependent on the strength of the electron confinement and the size of the system. In addition, although the most dominant factor that determines the charge decoherence rate is the energy splitting between the charge qubit states, the details of the double dot configuration is also very important.

PACS numbers: 03.67.Lx, 73.21.La, 85.35.Be, 63.20.Kr

I. INTRODUCTION

Ever since Peter Shor showed that a purely quantum mechanical computer can be used to achieve exponential speedup (compared to classical computers) in solving the prime factoring problem,¹ there has been widespread interests in the study of quantum information science in general, and in building a practical quantum computer in particular.^{2,3} Some of the most prominent proposals are based on solid state structures, whether superconducting nanocircuits^{4,5,6,7} or semiconductor nanostructures such as quantum dots and regular donor arrays.^{8,9,10,11,12,13} A major presumed advantage of these systems, especially the semiconductor artificial structures, are their potential scalability, supported by the powerful and advanced semiconductor industry.

The great interest in semiconductor-based quantum computer architectures has prompted extensive studies of a variety of physical properties of nanostructures that are relevant to single electron spin or charge degree of freedom.¹⁴ In the present paper we focus on the decoherence properties of a charge qubit in semiconductors.^{10,12,13} For a charge qubit based on a single electron in a semiconductor double quantum dot (QD), charge decoherence has two important channels: Coulomb interaction to the background charge fluctuation and electron-phonon interaction.^{15,16,17,18,19,20} The former decoherence channel is widely present in all nanostructures. Presumably it is due to coupling with defects in the system and is thus extrinsic. The latter, however, is intrinsic to any solid state host material for the charge qubit.

In the following we present our study of charge qubit decoherence caused by electron-phonon interaction in a horizontally coupled two-dimensional GaAs double quantum dot. In Section II, we identify the electronic states we are interested in, and clarify the relevant types of phonons and electron-phonon interactions involved. We then derive the various relaxation and dephasing rates for double-quantum-dot-trapped single electrons. In Section III and IV, we show our results on charge relaxation and dephasing rates for a variety of configurations and states, and discuss the physical pictures and implications. Section V presents a summary of our results and our conclusions.

II. THEORETICAL DESCRIPTION OF ELECTRON-PHONON INTERACTION

A. A single confined electron in two coupled quantum dots

In this study we consider gated lateral quantum dots in a AlGaAs/GaAs/AlGaAs quantum well (QW). The growth direction (z direction, or vertical direction) confinement is due to the higher bandgap of the barrier material of AlGaAs. The lateral confinement is produced by the electrostatic potential from surface metallic gates. In general, the vertical direction confinement length (~ 10 nm) is much smaller than the lateral confinement length (50 nm), so that we can safely treat the dynamics along vertical and horizontal directions as decoupled. The system Hamiltonian (within the effective mass and envelope function approximations) is thus

$$\hat{\mathcal{H}} = \hat{\mathcal{H}}_{\parallel} + \hat{\mathcal{H}}_z, \quad (1)$$

where the growth direction component $\hat{\mathcal{H}}_z$ takes the form

$$\hat{\mathcal{H}}_z = -\frac{\hbar}{2}\partial_z \frac{1}{m^*(z)}\partial_z + V_0\Theta\left(|z| - \frac{L_z}{2}\right). \quad (2)$$

Here $m^*(z)$ is the electron effective mass and V_0 the offset between the band edges of the GaAs well and the AlGaAs barrier. For simplicity, we take the z -direction wavefunction as the wavefunction of an infinite QW ($V_0 \rightarrow \infty$). In this work, we do not consider excitations along z -direction because of the much higher excitation energy (compared to the lateral direction), so that the z -direction wavefunction is always given by $\psi_z(z) = \mathcal{A} \cos(\pi z/2L_z)$ where \mathcal{A} is a coefficient to be determined by normalization and $2L_z$ is the width of the QW.

The lateral confinement is assumed to be parabolic for a single QD, so that a single electron Hamiltonian in the lateral direction is

$$\hat{\mathcal{H}}_{\parallel} = -\frac{\hbar^2}{2m^*}\nabla^2 + \frac{1}{2}m^*\omega_0^2 r_{\parallel}^2 \quad (3)$$

where ω_0 describes the strength of the harmonic confinement in the $x - y$ plane. The total electron wavefunction can now be written as a product of

$$\psi(\mathbf{r}) = \psi_{\parallel}(\mathbf{r}_{\parallel}) \psi_z(z) \quad (4)$$

In the case of a single QD, the two-dimensional (2D) one-electron wavefunctions are essentially 2D harmonic oscillator functions^{21,22} and are described in terms of the principal quantum number $n = 0, 1, 2, \dots$ and the angular momentum quantum number $m = 0, \pm 1, \pm 2, \dots$ as

$$\psi_{\parallel}^{(n,m)}(\tilde{\rho}, \theta) = \sqrt{\frac{n!}{\pi l^2 (n+|m|)!}} \tilde{\rho}^{|m|} e^{-\tilde{\rho}^2/2} e^{im\theta} \mathcal{L}_n^{|m|}(\tilde{\rho}^2) \quad (5)$$

where $\mathcal{L}_n^{|m|}(\tilde{\rho}^2)$ are the Laguerre polynomials, and $\tilde{\rho} = |\mathbf{r}_{\parallel}|/l$ is a scaled radius, with $l = \sqrt{\hbar/m^*\omega_0}$. The corresponding eigenvalues are

$$E_{nm} = (2n + |m| + 1) \hbar\omega_0. \quad (6)$$

For two QDs that are horizontally coupled, we use a simple in-plane confinement of two parabolic wells separated by an inter-dot distance 2α :

$$V_c = \frac{1}{2}m^*\omega_0^2 \min\{(x - \alpha)^2 + y^2, (x + \alpha)^2 + y^2\} \quad (7)$$

The single electron wavefunction for the lateral direction is, in general, given by a superposition of the single-dot wavefunctions:

$$|\Psi_{\parallel}\rangle = \sum_k C_k |\psi_{\parallel,L}^k\rangle + D_k |\psi_{\parallel,R}^k\rangle, \quad (8)$$

and the total wavefunction of the system of the coupled QDs is

$$\Psi(\mathbf{r}) = \Psi_{\parallel}(\mathbf{r}_{\parallel}) \psi_z(z) \quad (9)$$

Notice that for charge qubits there is only a single electron in a double dot, in contrast with spin qubits, where each quantum dot has an electron and double dot is only for two-qubit operations.^{8,23} In the present study, the wavefunctions for the coupled-QD are calculated numerically by direct diagonalization, using reasonable parameters of a GaAs QW.

B. Electron-Acoustic phonons coupling

In a polar semiconductor like GaAs, electrons couple to all types of phonons. More specifically, in GaAs electrons couple to longitudinal acoustic phonons through a deformation potential, to longitudinal and transverse acoustic

	m/m_e	D (eV)	c_s (m/s)	ρ (Kgr/m ³)	e_{14} (V/m)	ϵ_s	ϵ_∞	ω_{LO} (meV)	ω_{TO} (meV)
GaAs	0.067	8.6	3700	5300	1.38×10^9	12.9	10.89	36.25	33.29

TABLE I: Material parameters (m_e is the electron mass).

phonons through piezoelectric interaction, and to the optical phonons through the polar interaction.²⁴ The deformation potential electron-phonon interaction is given by

$$H_D = D \sum_{\mathbf{q}} \left(\frac{\hbar}{2\rho_m V \omega_{\mathbf{q}}} \right)^{1/2} |\mathbf{q}| \rho(\mathbf{q}) (a_{\mathbf{q}} + a_{-\mathbf{q}}^\dagger), \quad (10)$$

where D is the deformation constant, ρ_m is the mass density of the host material, V is the volume of the sample, $a_{\mathbf{q}}$ and $a_{-\mathbf{q}}^\dagger$ are phonon annihilation and creation operators, and $\rho(\mathbf{q})$ is the electron density operator. Table I presents the material parameters used in our numerical calculation.

Electrons can interact also with longitudinal and transverse acoustic phonons through piezoelectric interaction. This type of interaction is essentially due to the lack of symmetry of in the crystal, thus for materials like Si, which has crystal inversion symmetry, the piezoelectric interaction is not present. On the other hand, the crystal of GaAs lacks inversion symmetry, so piezoelectric interaction is nonvanishing. The electric displacement \mathcal{D} is related to the electric field \mathcal{E} , strain S , and the permitivity tensor ϵ in a piezoelectric crystal by²⁵

$$\mathcal{D}_i = \sum_i \epsilon_{ij} \mathcal{E}_j + \sum_{k,l} e_{ikl} S_{kl} \quad (11)$$

where the third rank tensor e_{ikl} is the piezoelectric constant tensor. As a result, the electron-phonon coupling due to the piezoelectric effect is²⁴

$$H_P = i \sum_{\mathbf{q}} \left(\frac{\hbar}{2\rho_m V \omega_{\mathbf{q}}} \right)^{1/2} \mathcal{M}_{\lambda}^{pz}(\hat{q}) \rho(\mathbf{q}) (a_{\mathbf{q}} + a_{-\mathbf{q}}^\dagger) \quad (12)$$

where λ denotes polarization of the acoustic phonons. In the case of zincblende crystals there is only one independent and nonvanishing piezoelectric constant: $e_{14} = e_{25} = e_{36}$, so that the matrix element $\mathcal{M}_{\lambda}^{pz}$ is given by^{24,26,27}

$$\mathcal{M}_{\lambda}^{pz}(\hat{\mathbf{q}}) = 2e e_{14} (\hat{q}_x \hat{q}_y \xi_z + \hat{q}_y \hat{q}_z \xi_x + \hat{q}_x \hat{q}_z \xi_y) \quad (13)$$

where ξ denotes the unit polarization vector and e is the electron charge.

Notice that the Hamiltonian for deformation potential and piezoelectric interaction are real and imaginary, respectively, which allow us to investigate separately these interactions and calculate the total contribution by simply adding up the two rates.²⁴

C. Electron-Optical phonons coupling

Even though the electronic energy involved in the study of charge qubits is generally quite small (a few meV) compared to the optical phonon energy (~ 36 meV in GaAs), we will demonstrate later that electron-optical-phonon interaction does play a role in the decoherence of electron orbital states. For the purpose of this calculation, we will use the simple polar interaction in the bulk, neglecting the more intricate details involving heterostructures.^{28,29,30} The electron-phonon interaction due to LO phonons is thus given by²⁴

$$H_{OP} = \sum_{\mathbf{q}} \frac{M}{q\sqrt{V}} \rho(\mathbf{q}) (a_{\mathbf{q}} + a_{-\mathbf{q}}^\dagger) \quad (14)$$

and

$$M^2 = 2\pi e^2 \hbar \omega_{LO} \left(\frac{1}{\epsilon_\infty} - \frac{1}{\epsilon_s} \right) \quad (15)$$

in which ω_{LO} is the longitudinal optical frequencies, ϵ_s and ϵ_∞ are the static and high frequency dielectric constant.

Now that we have identified all the electron-phonon interaction involved in our system, we are ready to study what concrete forms they take in a double quantum dot system, and evaluate the dephasing and relaxation rates for an electron in a double quantum dot due to its interaction with the phonons.

III. RELAXATION AND DEPHASING RATES DUE TO ELECTRON-PHONON INTERACTION

A. Electron-phonon coupling in a double quantum dot

Before performing numerical evaluations of the electron charge relaxation and dephasing rates, we first clarify the physical picture of charge decoherence in a double quantum dot. As an example and without loss of generality, let us examine the deformation potential electron-phonon interaction given by Eq. (10) in which $\rho(\mathbf{q})$ is the Fourier transform of the electron density operator:

$$\rho(\mathbf{q}) = \sum_{\kappa, \eta} c_{\kappa}^{\dagger} c_{\eta} \int d\mathbf{r} e^{-i\mathbf{q} \cdot \mathbf{r}} \phi_{\kappa}^*(\mathbf{r}) \phi_{\eta}(\mathbf{r}), \quad (16)$$

where κ and η are indices of electronic states, c_{κ} and c_{κ}^{\dagger} are electronic annihilation and creation operators for the κ -state, while ϕ are the electron wavefunctions. In the context of a coupled double QD, we can choose the double dot eigenstates as the basis for the single electron. For the two lowest-energy double-dot states Φ_{\pm} , which are chosen as the charge qubit basis states, κ and η take the values of $+$ and $-$ (from now on, these two states will be equivalently referred to as the ground and first excited states of the double dot, or the charge qubit states). The electron-phonon coupling Hamiltonian can then be conveniently written in this quasi-two-level basis in terms of the Pauli spin matrices σ_x and σ_z (where spin up and down states refer to the two electronic eigenstates):

$$\begin{aligned} H_D &= D \sum_{\mathbf{q}} \left(\frac{\hbar}{2\rho_m V \omega_{\mathbf{q}}} \right)^{1/2} |\mathbf{q}| (A_r(\mathbf{q}) \sigma_x + A_{\varphi}(\mathbf{q}) \sigma_z) (a_{\mathbf{q}} + a_{-\mathbf{q}}^{\dagger}), \\ A_r(\mathbf{q}) &= \langle -|e^{i\mathbf{q} \cdot \mathbf{r}}|+ \rangle, \\ A_{\varphi}(\mathbf{q}) &= \frac{1}{2} (\langle +|e^{i\mathbf{q} \cdot \mathbf{r}}|+ \rangle - \langle -|e^{i\mathbf{q} \cdot \mathbf{r}}|- \rangle). \end{aligned} \quad (17)$$

Since the basis for the quasi-two-level system are electron eigenstates for the double dot, the term proportional to σ_x above leads to transition between the two electronic eigenstates and causes relaxation. On the other hand, the term proportional to σ_z does not mix the electronic states, so that it only causes fluctuations in the energy splitting between the two electronic levels. Therefore it only leads to pure dephasing between the two electronic charge states, but not to relaxation.

For a discussion of the qualitative behavior of the electron-phonon coupling in a double dot, we first analyze the simple situation where the two dots are well separated and not strongly biased, so that only the two single-dot ground orbital states are involved. The relevant single-electron double-dot states are then

$$\Phi_+ = a\phi_A(\mathbf{r}) + b\phi_B(\mathbf{r}); \quad \Phi_- = b\phi_A(\mathbf{r}) - a\phi_B(\mathbf{r}), \quad (18)$$

with $\phi_{A(B)}(\mathbf{r}) = \varphi(\mathbf{r} - \mathbf{R}_{A(B)}) u_0(\mathbf{r})$, where $\varphi(\mathbf{r})$ is a slowly varying envelope function, and the Bloch function at the conduction band minimum ($\mathbf{k} = 0$ at Γ point) is equal to the periodic part $u_0(\mathbf{r})$. Though we have chosen the envelopes φ centered at each well to be identical, they could as well be different, as is generally the case for quantum dots. For small energy splittings between the Φ_{\pm} states, the fast oscillatory Bloch function $u_0(\mathbf{r})$ can be integrated separately, so that the matrix element A_r can be written as¹⁸:

$$\begin{aligned} A_r(\mathbf{q}) &= (ab^* - a^*b e^{i\mathbf{q} \cdot \mathbf{R}}) \int d\mathbf{r} e^{i\mathbf{q} \cdot \mathbf{r}} [\varphi(\mathbf{r})]^2 \\ &\quad + (|b|^2 - |a|^2) \int d\mathbf{r} e^{i\mathbf{q} \cdot \mathbf{r}} \varphi(\mathbf{r}) \varphi(\mathbf{r} - \mathbf{R}). \end{aligned} \quad (19)$$

Here the first integral is an on-site contribution modified by the phase difference $e^{i\mathbf{q} \cdot \mathbf{R}}$ between the two dots, while the second integral is a two-dot contribution that is generally much smaller because of the small interdot overlap.

The dephasing matrix element A_{φ} can be similarly calculated and the result is¹⁸

$$\begin{aligned} A_{\varphi}(\mathbf{q}) &= i (|b|^2 - |a|^2) e^{i\mathbf{q} \cdot \mathbf{R}/2} \sin \frac{\mathbf{q} \cdot \mathbf{R}}{2} \int d\mathbf{r} e^{i\mathbf{q} \cdot \mathbf{r}} [\varphi(\mathbf{r})]^2 \\ &\quad + (a^*b + ab^*) \int d\mathbf{r} e^{i\mathbf{q} \cdot \mathbf{r}} \varphi(\mathbf{r}) \varphi(\mathbf{r} - \mathbf{R}). \end{aligned} \quad (20)$$

Here the prefactors $|b|^2 - |a|^2$ and $a^*b + ab^*$ are for intradot and interdot integrals, exactly the opposite to those in Eq. (19).

Equations 19 and 20 clearly demonstrates that electron-phonon interaction induced electron charge decoherence is dominated by relaxation when $|b| \sim |a|$ so that A_φ is small,^{19,20} and by pure dephasing when $|b|$ and $|a|$ are very different (so that, for example, $|b| \sim 1$ and $|a| \sim 0$).²⁰ In other words, if the energy levels of the two quantum dots are close to resonance, relaxation matrix element is much larger than pure dephasing matrix element; while when the two single-dot levels are biased, relaxation is suppressed. These qualitative trends will persist even when we consider more realistic electron eigenstates as studied in section II.A. The argument here is based on the assumption that the off-site contributions are small because of a small wavefunction overlap between the two dots. Obviously, if the overlap is larger, the above trend becomes weaker.

B. Relaxation rates

The electron relaxation rates associated with phonon emission (or absorption) can be evaluated using Fermi's golden rule:

$$\Gamma = \frac{2\pi}{\hbar} \sum_{\mathbf{q}} \left| \left\langle \Psi^{(F)}(\mathbf{r}) \left| H^{int} \right| \Psi^{(I)}(\mathbf{r}) \right\rangle \right|^2 \delta(E_F - E_I \pm E_{\mathbf{q}}) \\ \left(N_B(E_{\mathbf{q}}, T_{lat}) + \frac{1}{2} \pm \frac{1}{2} \right) \quad (21)$$

Here labels 'I' and 'F' refer to the initial and final electron orbital states respectively, the plus (minus) sign denotes emission (absorption) of a phonon, and N_B is the Bose-Einstein distribution for phonons with lattice temperature T_{lat} (our calculations presented in this paper are all done at $T_{lat} = 0$, when phonon absorption can be neglected.).

Due to their large energies (~ 36 meV for LO phonons in GaAs), optical phonons do not contribute to electron orbital relaxation in a quantum dot except for the highly excited states, which are irrelevant for the context of charge-based quantum computing. Therefore, the only phonons that contribute to electron relaxation here are acoustic phonons.³¹

C. Pure dephasing rates

Relaxation is not the only way charge qubits can be decohered. If the energy difference between the two charge states fluctuates, phase information will get lost and decoherence occurs. Such pure dephasing (in the sense that no transition occurs between the two charge states) due to a bosonic bath has been calculated before.^{35,36} Pure dephasing due to electron-acoustic-phonon interaction has also been evaluated for spherical quantum dots and donors in semiconductors.²⁰ The density operator of an electron in a boson bath can be written in a general expression as

$$\rho(t) = \begin{pmatrix} \rho_{00}(0) & \rho_{01}(0)e^{-B^2(\Delta t)+i\varepsilon\Delta t/\hbar} \\ \rho_{10}(0)e^{-B^2(\Delta t)-i\varepsilon\Delta t/\hbar} & \rho_{11}(0) \end{pmatrix} \quad (22)$$

where ε is the energy splitting between the electron energy levels. In short, pure dephasing cause a decay in the off-diagonal element of the density matrix for the two-level system that makes up the charge qubit^{20,35,36}:

$$\rho_{01}(t) \sim \rho_{01}(0)e^{-B^2(t)}, \quad (23)$$

where the exponent function $B^2(t)$ is defined by

$$B^2(t) = \frac{V}{\hbar^2 \pi^3} \int d^3 \mathbf{q} \frac{|g(\mathbf{q})|^2}{\omega_{\mathbf{q}}^2} \sin^2 \frac{\omega_{\mathbf{q}} t}{2} \coth \frac{\hbar \omega_{\mathbf{q}}}{2k_B T}. \quad (24)$$

Here $\omega_{\mathbf{q}}$ is the frequency of the phonons. In our study, we have investigated dephasing effects due to both acoustic and optical phonons. For acoustic phonons, we choose $\omega_{\mathbf{q}} = qc_s$ for the relevant branches, while for longitudinal optical phonons, we choose $\omega_{\mathbf{q}} = \omega_{LO}$. It can be shown straightforwardly that the phonons that contribute significantly to pure dephasing are zone-center phonons (small $|\mathbf{q}|$ values), so that choosing linear and constant dispersion for acoustic and optical phonons is an excellent approximation. The coupling constants $g(\mathbf{q})$ due to deformation potential, piezoelectric and optical phonons are respectively given by

$$g_{\text{def}}(\mathbf{q}) = D \sqrt{\frac{\hbar q}{2\rho c_s V}} \mathcal{I}(\mathbf{q}), \quad (25)$$

$$g_{\text{piezo}}(\mathbf{q}) = \mathcal{M}_\lambda^{pz}(\mathbf{q}) \sqrt{\frac{\hbar}{2\rho c_s V}} \mathcal{I}(\mathbf{q}), \quad (26)$$

$$g_{\text{polar}}(\mathbf{q}) = \frac{M}{q\sqrt{V}} \mathcal{I}(\mathbf{q}), \quad (27)$$

where $\mathcal{I}(\mathbf{q})$ is defined by

$$\mathcal{I}(\mathbf{q}) = \frac{1}{2} (\langle \Psi^-(\mathbf{r}) | e^{\mp i\mathbf{q}\cdot\mathbf{r}} | \Psi^-(\mathbf{r}) \rangle - \langle \Psi^+(\mathbf{r}) | e^{\mp i\mathbf{q}\cdot\mathbf{r}} | \Psi^+(\mathbf{r}) \rangle) = -A_\varphi(\mathbf{q}). \quad (28)$$

Here \pm refer to the two states for the double dot charge qubit. Notice that all the integrals in this study are carried out using the Monte-Carlo technique.

IV. RESULTS AND DISCUSSIONS

A. Charge relaxation due to acoustic phonons

We first calculate the electron relaxation rate from the excited charge qubit state (the first excited state of the double quantum dot) and explore its behavior as a function of the double dot parameters such as interdot distance and strength of the single dot confinement. Notice that throughout this paper, the QW width takes on a fixed value of $2L_z = 6$ nm. We have also done calculations for a well width of 10 nm and the results are only slightly different.

Figure 1 shows the electron relaxation rate as a function of the interdot distance for an electron that is initially in the first excited state. The relaxation process is dominated by the emission of one acoustic phonon. For small inter-dot separations, the contribution due to deformation potential interaction is larger than due to piezoelectric interaction. For larger inter-dot separation, however, piezoelectric coupling becomes the dominant contributor because of the different wavevector dependence in the deformation and piezoelectric matrix elements (\sqrt{q} for deformation potential versus $1/\sqrt{q}$ for piezoelectric interaction). Since phonon density of state goes to zero at small energy $\propto E^2$, the relaxation rate decreases with decreasing energy splitting between the initial and final states, which is the case for both very shallow confinement wells and for largely separated quantum dots. Experimentally, it has been found¹⁵ that for large dots and large interdot distance (~ 150 nm) relaxation rates due to electron-phonon coupling should be smaller than 10^9 s⁻¹. Our calculations are quite consistent with these experimental observations.

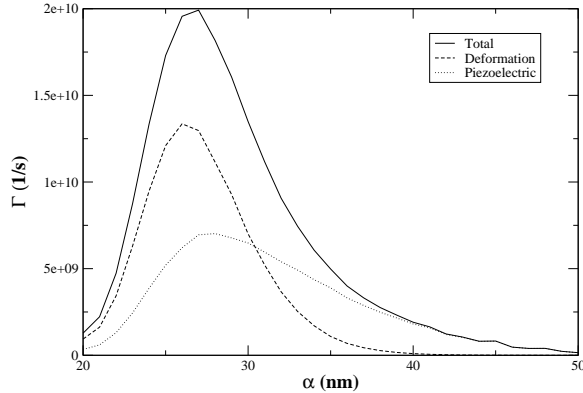


FIG. 1: Relaxation rates of an electron in the first excited state through acoustic phonon emission as a function of the half interdot distance α . The relaxation rates due to deformation potential interaction, piezoelectric interaction, and the total relaxation rates are presented by dashed, dotted, and straight lines respectively. The strength of the lateral confinement is $\hbar\omega_0 = 3$ meV.

In Fig. 2 we plot the dependence of the relaxation rates on the confinement strength of one of the quantum dots (they are considered to be identical in this problem) for a fixed interdot distance of $2\alpha = 60$ nm. The relaxation rates increase with increasing confinement strength as the energy splitting between the first excited state and the ground state increases (as illustrated by the inset of Fig. 3), until the confinement strength reaches about $\hbar\omega \simeq 2.4$ meV.

Further increase in confinement strength causes increase of interdot barrier and a decrease in energy separation of the charge qubit states, so that relaxation rates also decrease as a consequence of the reducing energy splitting. The differences between the contributions of the two different types of electron-phonon interactions can again be interpreted in the same manner as in Fig. 1. The relaxation rates can also be given as a function of the energy splitting between

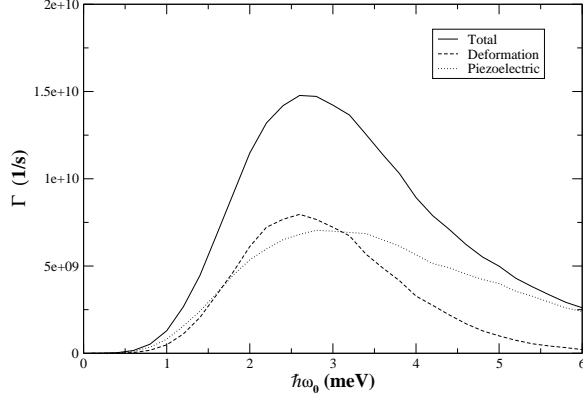


FIG. 2: The relaxation rates versus the strength of the confinement. The scattering rates due to deformation potential, piezoelectric phonons and total relaxation rates are presented by dashed, dotted and straight line respectively. The interdot distance is $2\alpha = 60$ nm.

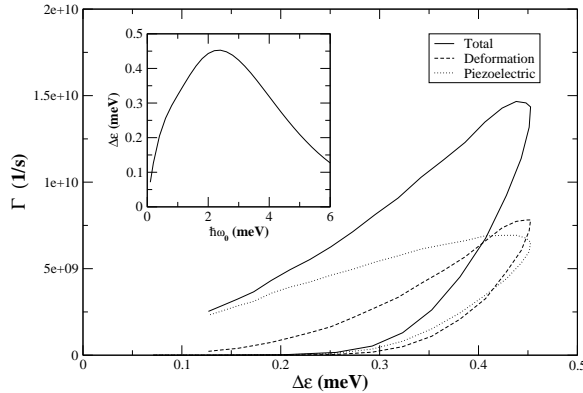


FIG. 3: Electron relaxation rates as a function of the energy splitting between the first excited state and the ground state in a double quantum dot. Again, rates due to deformation potential, piezoelectric interaction, and the total relaxation rates are represented by dashed, dotted, and straight line respectively. The energy splitting versus the confinement strength is given in the inset. The interdot distance is $2\alpha = 60$ nm.

the first excited state and the ground state ($\Delta\epsilon$), as presented in Fig. 3. Theoretically this graph more directly reveals the behavior of the relaxation rates: that it decreases monotonically with decreasing energy splitting between the initial and final states, basically because of the fast decreasing phonon density of state. In the double dot situation we study here for each energy splitting there could be two different dot configurations, as illustrated in the inset, thus there are two branches for Fig. 3. Notice that the energy splitting dependence of the relaxation rates is not universal,¹⁶ because the electron-phonon matrix elements do sensitively depend on the form/size of the electron wavefunctions.

Since we have calculated the low energy spectrum of a horizontally coupled double quantum dot, we can easily calculate phonon emission rates when the electron is in an excited state. For example, Fig. 4 presents the phonon emission rates of an electron initially in the second excited state as a function of the half interdot dot distance α . Now a phonon-emitting transition can take the electron to either the first excited or the ground state. Furthermore, since the second excited state of a double dot is essentially made up of the $2p$ orbitals of the two single quantum dots, the energy splitting between the second excited and the first excited or ground states never goes to zero: at large

interdot separation, this energy splitting approaches single electron excitation energy $\hbar\omega_0$, which is chosen as 3 meV in this calculation. Thus the phonon emission rate remains finite at large interdot separation, as clearly illustrated in Fig. 4. In essence now electron relaxation is dominated by the electron-phonon coupling in each of the single quantum dots. This also explains why the relaxation rates into the first excited state and the ground state becomes identical as interdot separation increases.

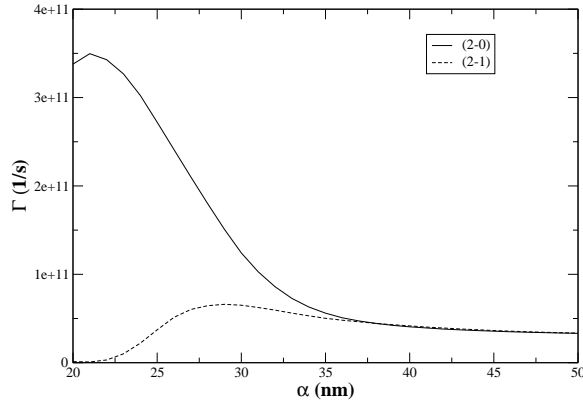


FIG. 4: The relaxation rates for the second excited state as a function of the half interdot distance α . The total scattering rates include contributions from both the deformation potential and the piezoelectric interaction. The straight line gives relaxation rates to the ground state, while the dashed line is the relaxation rates to the first excited state. The strength of the confinement is $\hbar\omega_0 = 3$ meV.

In summary, our results on the electron relaxation through single phonon emission in a double quantum dot³⁷ show a relatively simple and straightforward dependence on energy separation of the initial and final states (basically related to phonon density of state), and thus a sensitive dependence on the confinement strength and interdot distance (since energy splitting between the charge qubit states depends sensitively on these parameters). According to Eq. 19 there is a strong angular dependence for the electron-phonon coupling matrix elements. However, integral over the phonon wavevectors essentially averages out all the detailed features in the final relaxation rates. Another feature of our results is that piezoelectric interaction dominates when the energy splitting between the charge qubit states is small, while deformation potential interaction dominates when the energy splitting is large. This feature again has a very simple physical explanation in the different \mathbf{q} -dependence of the two types of interaction.

B. Pure charge dephasing due to acoustic and optical phonons

Electron-phonon interaction not only causes electron relaxation (or excitation at finite temperatures) between qubit states, it can also cause dephasing between them if the electron is in a superposition state, as we have discussed in Section III.C. Here we calculate the dephasing effects from both acoustic and optical phonons. According to Eqs. (23) and (24), the quantity $B^2(t)$ completely determines the loss of coherence from the off-diagonal density matrix element between the charge qubit states, therefore it is the quantity we focus on in all the results and figures in the following.

Figure 5 presents the time dependence of dephasing between the charge qubit states for an unbiased system due to acoustic phonons. According to Eq. (20), dephasing should be quite small in the unbiased situation because it mostly comes from overlaps in between the double dot. An interesting feature of curves in Fig. 5 is that they rapidly increase for the first 10 ps or so, then more or less saturate, so that $B^2(t)$ depends only very slowly on time after 100 ps. Mathematically, the very fast time-dependence of dephasing is due to the trigonometric dependence on phonon frequencies and time $\sin\omega_s t/2$. As indicated in Eq. (20), only zone-center phonons contribute significantly to dephasing (because of the integral over $\exp(i\mathbf{q} \cdot \mathbf{r})$), with frequency ranging from zero up to $\sim \hbar c_s/\alpha$, which is in the order of 0.1-1 THz for GaAs. As time evolves starting from zero, the zone-center phonon contributions quickly mix and the initial rise of $B^2(t)$ is mostly determined by the higher frequency phonons because their density of state is much higher. After the initial rise, phonons with different frequencies will not contribute always constructively, thus producing the much flatter behavior of $B^2(t)$. Furthermore, $B^2(t)$ will not rise monotonically after the initial rise because the phonons contribute through a sinusoidal function. The time evolution shows that dephasing quickly rises but then saturates after about 100 ps.

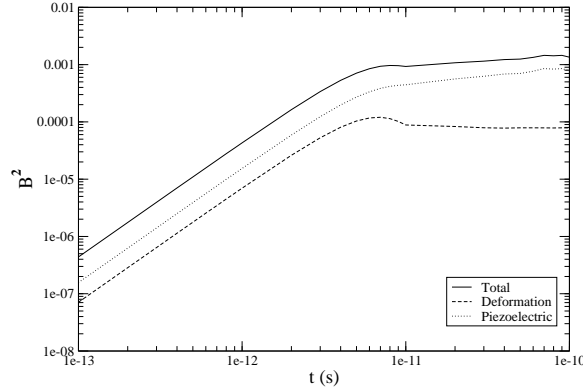


FIG. 5: Dephasing rates as a function of time t . The dashed, dotted, and straight lines represented dephasing rates due to deformation potential, piezoelectric interaction, and the total, respectively. The strength of the confinement $\hbar\omega_0 = 3$ meV, the interdot distance is $2\alpha = 60$ nm, and there is no interdot bias: $V_R = 0$ meV.

The dephasing behavior here is quite different from the ordinarily assumed $\exp(-\gamma_p ht)$ type of behavior. This difference is closely related to the spin-boson type of coupling in the present problem^{35,36} and to a degree the phonon density of state of the semiconductor structure. There are two important consequences for the temporal behavior of $B^2(t)$. First, there is a very fast initial dephasing, occurring in a time period smaller than 100 ps, due to the interaction between the qubit electron and the acoustic phonon bath. Second, the time-dependence of B^2 at large time is very flat—it can basically be taken as a constant after 100 ps. A constant dephasing factor will not produce a decaying signal in terms of, for example, oscillations in electrons. Instead, it simply reduces the contrast in the charge oscillation. This can be seen easily from Eq. 22. The presence of a constant $\exp(-B^2) \sim \exp(-0.05)$ simply reduces the magnitude of ρ_{01} by a constant factor of 0.05, which is not a particularly large suppression (though significant in terms of fault tolerant quantum computing).

In Fig. 6 we further explore the dephasing rates as a function of the interdot distance for an unbiased system. As indicated in Eq. (20), if the two quantum dot are well separated, the overlap integrals go down quickly, so that dephasing should also be strongly suppressed. This is exactly the behavior we observe in Fig. 6.

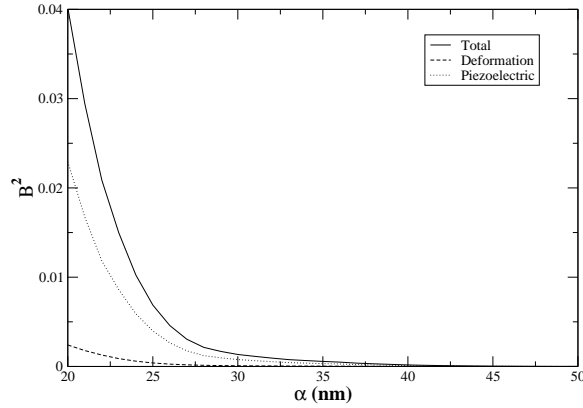


FIG. 6: Dephasing factor $B^2(t)$ as a function of the half interdot distance α . No bias is applied across the two quantum dots, and time t is chosen to be 60 ps. The dephasing rates due to deformation potential, piezoelectric interaction, and total dephasing rates are represented by dashed, dotted, and straight line respectively. The strength of the confinement is $\hbar\omega_0 = 3$ meV.

When a bias is applied between the two quantum dots of the double dot, the magnitude of dephasing should increase, which is exactly what our numerical results presented in Figs. 7 and 8 follow. Figure 7 shows a very similar temporal behavior as that in the unbiased cases, albeit with a much larger saturated value for B^2 . Figure 8 shows

the dependence on the interdot bias voltage V_R by the dephasing rate. As expected from Eq. (20), the dephasing rates increases but then saturates as the qubit states at high bias are essentially the two single dot ground states (assuming higher excited states still have not influenced the charge qubit states yet). In Fig. 8 we have also included the contribution of optical phonons to dephasing. Although this contribution is smaller than the acoustic phonon effect, it is still a considerable contribution.

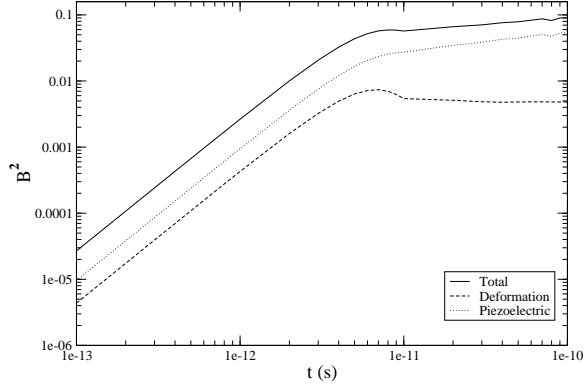


FIG. 7: Dephasing rates as a function of time t in the presence of interdot bias. Again, the dephasing rates due to deformation potential, piezoelectric interaction, and the total rates are represented by dashed, dotted, and straight line respectively. The strength of the confinement is $\hbar\omega_0 = 3$ meV, the interdot distance is $2\alpha = 60$ nm, and the interdot bias voltage is $V_R = 1.5$ meV.

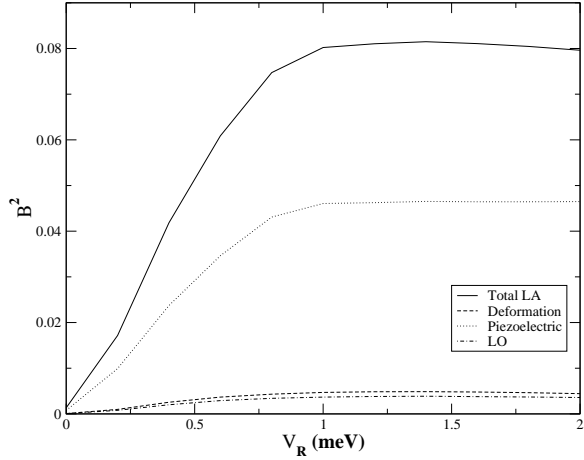


FIG. 8: Dephasing rates as a function of the interdot bias voltage V_R . The solid line represents dephasing rates due to electron-acoustic-phonon interaction through both deformation potential and piezoelectric interaction. The dashed and dotted lines represent the deformation potential and piezoelectric contributions separately. The dot-dashed line represents the dephasing effects from polar interaction with optical phonons. Here the strength of the confinement is $\hbar\omega_0 = 3$ meV, the interdot distance is $2\alpha = 60$ nm, and the time of observation for the dephasing effect is $t = 60$ ps.

As we have pointed out before, optical phonons do not contribute significantly to electron relaxation. However, the zone-center longitudinal optical phonons do contribute to dephasing through the polar interaction. To better understand the pure dephasing due to the electron polar interaction with optical phonons, we can perform an analytical assessment for a simple double dot configuration. For optical phonons, $\omega_{\mathbf{q}} = \omega_{LO}$ is a constant near the zone center. Thus at zero temperature

$$B^2(t) = \frac{M^2}{\pi^3(\hbar\omega_{LO})^2} \sin^2 \frac{\omega_{LO}t}{2} \int d^3\mathbf{q} \frac{|\mathcal{I}(\mathbf{q})|^2}{q^2}$$

$$= \frac{2e^2}{\pi^2 \hbar \omega_{LO}} \left(\frac{1}{\epsilon_\infty} - \frac{1}{\epsilon_0} \right) \sin^2 \frac{\omega_{LO} t}{2} \int dq d\Omega |\mathcal{I}(\mathbf{q})|^2 \quad (29)$$

The q -integral is now just a number that is inversely proportional to the size of the double dot. The magnitude of B^2 is thus determined by the polar interaction strength and the double dot size, and the time-dependence of B^2 is all in the sinusoidal factor. Therefore, pure dephasing due to optical phonons sets in at a very small time scale, in the order of 100 femtoseconds because of the fact that $\hbar \omega_{LO} \sim 36$ meV. The magnitude of B^2 is not vanishingly small, either. Using nominally GaAs parameters and assume spherical quantum dots with Gaussian wavefunctions $\sim \exp(-r^2/2a^2)$, we can estimate the order of magnitude of the dephasing factor as

$$\begin{aligned} B^2(t) &\approx \frac{4\sqrt{2}(e^2/a)}{\sqrt{\pi} \hbar \omega_{LO}} \left(\frac{1}{\epsilon_\infty} - \frac{1}{\epsilon_0} \right) \sin^2 \frac{\omega_{LO} t}{2} \\ &\sim 0.05 \sin^2 \frac{\omega_{LO} t}{2}. \end{aligned} \quad (30)$$

For the last step we assume a wavefunction size $a \sim 20$ nm, which corresponds to a pretty small quantum dot. Since B^2 is inversely proportional to the size a of the quantum dot wavefunction, larger quantum dot would produce a smaller dephasing magnitude for B^2 . Anyway, it is clear that optical phonons produce a dephasing effect that has a comparable if somewhat smaller magnitude as the acoustic phonons.

The dephasing effect from optical phonons evolves extremely fast, so that the only observable effect would be its average over time, which is a constant. This is quite similar to the pure dephasing effect from the acoustic phonons, which also rises rapidly (~ 100 ps, slower than optical phonons but still much faster than the ordinary time scale of nanosecond for charge dynamics). Recall that a constant dephasing factor will only reduce the contrast in the measurable quantities such as charge oscillation. For optical phonons this amounts to a reduction in the magnitude of ρ_{01} by a constant factor of 0.95, which, like for acoustic phonons, is not a large suppression. Experimental techniques have not developed to the degree to allow detection of such a small suppression of signals.

In short, dephasing effects on the electron orbital degrees of freedom from electron-phonon interaction in a double dot should reveal itself mostly through a reduction of contrast in measurable physical quantities (such as electron oscillation between the double dot), but not a temporally decaying signal. Decays observed in experiments such as 15 should originate from relaxation, not dephasing, if it is dominated by electron-phonon interaction.

V. CONCLUSIONS

In this study we have investigated electron decoherence in a double quantum dot due to electron-phonon coupling. In particular, we have evaluated electron relaxation through emission of a single acoustic phonon. We found a sensitive dependence of the relaxation rates on system parameters such as confinement strength and interdot distance. We have also evaluated electron dephasing through interaction with both acoustic and optical phonons—because of the absence of energy conservation requirement, all phonon modes contribute to dephasing.

VI. ACKNOWLEDGMENT

The work is supported in part by NSA and ARDA under ARO contract No. DAAD19-03-1-0128.

¹ P.W. Shor, in *Proceedings of the 35th Annual Symposium on the Foundations of Computer Science*, ed. by S. Goldwasser (IEEE Computer Society, Los Alamitos, 1994), p. 124.

² D. DiVincenzo, *Science* **270**, 255 (1995); A. Steane, *Rep. Prog. Phys.* **61**, 117 (1998); I. Žutić, J. Fabian, and S. Das Sarma, *Rev. Mod. Phys.* **76**, 323 (2004).

³ M. Nielsen and I.L. Chuang, *Quantum Computation and Quantum Information* (Cambridge, Cambridge 2000).

⁴ Yu. Makhlin, G. Schn, and A. Shnirman, *Rev. Mod. Phys.* **73**, 357-400 (2001).

⁵ V. Bouchiat, D. Vion, P. Joyez, D. Esteve, and M.H. Devoret, *Phys. Scripta T* **76**, 165 (1998).

⁶ Y. Nakamura, Yu.A. Pashkin, and J.S. Tsai, *Nature* **398**, 786 (1999).

⁷ I. Chiorescu, P. Bertet, K. Semba, Y. Nakamura, CJPM Harmans, and JE Mooij, *Science* **431**, 159 (2004).

⁸ D. Loss and D.P. DiVincenzo, *Phys. Rev. A* **57**, 120 (1998).

⁹ B.E. Kane, *Nature* **393**, 133 (1998); *Fortschr. Phys.* **48**, 1023 (2000).

¹⁰ T. Tanamoto, *Physica B* **272**, 45 (1999).

¹¹ M.S. Sherwin, A. Imamoglu, and T. Montroy, Phys. Rev. A **60**, 3508 (1999).

¹² L. Fedichkin, M. Yanchenko, and K.A. Valiev, Nanotechnology **11**, 387 (2000).

¹³ L.C.L. Hollenberg *et al.*, Phys. Rev. B **69**, 113301 (2004).

¹⁴ X. Hu and S. Das Sarma, Phys. Stat. Sol. (b) **238**, 260 (2003); X. Hu, cond-mat/0411012, a brief review on quantum dot quantum computing.

¹⁵ T. Hayashi, T. Fujisawa, H. D. Cheong, Y. H. Jeong, and Y. Hirayama, Phys. Rev. Lett. **91**, 226804 (2003).

¹⁶ T. Fujisawa, T. H. Oosterkamp, W.G. van der Wiel, B.W. Broer, R. Aguado, S. Tarucha, L. P.Kouwenhoven, Science **282**, 932 (1998).

¹⁷ S. Vorojtsov, E.R. Mucciolo, and H.U. Baranger, cond-mat/0412190.

¹⁸ X. Hu, B. Koiller and S. Das Sarma, cond-mat/0412340.

¹⁹ S. D. Barrett and G. J. Milburn, Phys. Rev. B **68**, 155307 (2003).

²⁰ L. Fedichkin and A. Fedorov, Phys. Rev. A **69**, 032311 (2004).

²¹ L. Jacak, P. Hawrylak, and A. Wójs, *Quantum Dots* (Springer, 1998).

²² U. Bockelmann Phys. Rev. B **50**, 17271 (1994).

²³ X. Hu and S. Das Sarma, Phys. Rev. A **61**, 062301 (2000).

²⁴ Gerald D. Mahan, *Many-Particle Physics* (Plenum Press, New York, 1990).

²⁵ B. K. Ridley, *Quantum processes in semiconductors* (Clarendon Press, Oxford, 1982).

²⁶ G. D. Mahan, in *Polarons in Ionic Crystals and Polar Semiconductors*, ed. J. T. Devreese (North-Holland, Amsterdam, 1972), pp.553-657.

²⁷ H. Bruus, K. Flensberg, and H. Smith Phys. Rev. B **48**, 11144 (1993).

²⁸ N. C. Constantinou, J. Phys.: Condens. Matter **3**, 6859 (1991); V. N. Stavrou, M Babiker, and C. R. Bennett J. Phys.: Condens. Matter **13**, 6489 (2001); V. N. Stavrou, C R Bennett, O.M.M. Al-Dossary, and M Babiker, Phys. Rev. B **63**, 205304 (2001).

²⁹ B. K. Ridley, *Electrons and Phonons in Semiconductor* (Cambridge University Press, 1996).

³⁰ V. N. Stavrou, Physica B-Condensed Matter **337**, 87 (2003).

³¹ In the present study we have only included the three-dimensional bulk acoustic phonons, but not two-dimensional surface acoustic waves^{16,32} or confined acoustic waves.^{33,34}

³² J.M. Shilton *et al.*, Phys. Rev. B **51**, R14770 (1995).

³³ M.A. Stroscio and K.W. Kim, Phys. Rev. B **48**, 1936 (1993).

³⁴ B.A. Glavin, V.I. Pipa, V.V. Mitin, and M.A. Stroscio, Phys. Rev. B **65**, 205315 (2002).

³⁵ G.M. Palma, K.A. Suominen, and A.K. Ekert, Proc. Roy. Soc. Lond A vol. 452, pp. 567-584, (1996).

³⁶ L.M. Duan and G.C. Guo, Phys. Rev. A **57**, 737 (1998).

³⁷ Our calculations presented in this paper are all done at $T_{lat} = 0$, when phonon absorption can be neglected. At finite lattice temperature, phonon absorption becomes finite. However, its behavior will not be significantly different from emission as it will also be dominated by zone center phonons and limited by the phonon density of states.